PHOTONICS Research

Exciton binding energy and effective mass of $CsPbCl_3$: a magneto-optical study

Michal Baranowski,[1] Paulina Plochocka,[1,2] Rui Su,[3] Laurent Legrand,[4] Thierry Barisien,[4] Frederick Bernardot,[4] Qihua Xiong,[3] Christophe Testelin,[4] and Maria Chamarro[4,*]

[1]Department of Experimental Physics, Faculty of Fundamental Problems of Technology, Wroclaw University of Science and Technology, Wroclaw, Poland
[2]Laboratoire National des Champs Magnétiques Intenses, UPR 3228, CNRS-UGA-UPS-INSA, Grenoble and Toulouse, France
[3]Division of Physics and Applied Physics, School of Physical and Mathematical Sciences, Nanyang Technological University, Singapore, Singapore
[4]Sorbonne Université, CNRS-UMR 7588, Institut des NanoSciences de Paris, INSP, Paris, France
*Corresponding author: maria.chamarro@insp.jussieu.fr

Received 9 July 2020; revised 10 August 2020; accepted 11 August 2020; posted 12 August 2020 (Doc. ID 401872); published 25 September 2020

High magnetic field spectroscopy has been performed on lead chloride-based perovskite, a material that attracts significant interest for photovoltaic and photonic applications within the past decades. Optical properties being mainly driven by the exciton states, we have measured the fundamental parameters, such as the exciton binding energy, effective mass, and dielectric constant. Among the inorganic halide perovskites, $CsPbCl_3$ owns the largest exciton binding energy and effective mass. This blue emitting compound has also been compared with lower band gap energy perovskites and other semiconducting phases, showing comparable band gap dependences for binding energy and Bohr radius.

https://doi.org/10.1364/PRJ.401872

1. INTRODUCTION

Halide perovskite semiconductors have emerged as promising materials for photovoltaic and optoelectronic applications. Within the last decade, the conversion efficiency of perovskite solar cells has jumped in an impressive manner from 3% to 25% [1–3]. These outstanding results have also fueled interest on these materials in other domains. As a direct band gap semiconductor, lead halide perovskite also exhibits excellent electronic and emission properties, very interesting for optoelectronic applications as lasers and photodiodes [4–7], photodetectors [8], or polaritonic devices [9–13]. In addition, the flexible synthesis of nanostructures, such as nanocrystals or nanoplatelets, offers numerous opportunities for their integration in quantum devices and the development of applications in the field of quantum optics [14–16].

Emission properties being driven by the excitonic state, a direct experimental determination of the exciton parameters such as binding energy, effective mass, and Landé factor, is of prime importance for current understanding and future technological applications. Indeed, the theoretical models describing the exciton fine structure or describing the exciton magnetic behavior are based on the direct knowledge of the exciton parameters [17–22]. From the experimental point of view, getting accurate values of the binding energy implies that we can perform and analyze spectroscopic studies on these materials based on techniques such as absorption, photoluminescence, or reflectivity. Once the excitonic parameters are deduced, they allow for the interpretation of results obtained in more complex optical experiments such as time-resolved or photo-induced Faraday rotation measurements [23,24]. From the point of view of applications, the binding energy has to be compared with the thermal energy at the device operating point; it will determine whether the exciton will be stable or dissociate into electron and hole free carriers. The exciton stability is also important for polaritonic devices and room temperature (RT) single photon sources or lasers, while, for photovoltaic devices, the exciton dissociation is more interesting.

Here, we center our study on $CsPbCl_3$ bulk material, which shows the highest energy absorption edge in the family of the all-inorganic lead halide perovskites ($CsPbX_3$ with X = Cl, Br, or I). Recently, lasers and polaritonic effects have been evidenced in this material [9,25,26]. Moreover, nanostructured $CsPbCl_3$ materials extend the emission energy to the ultraviolet range and allow for considering the realization of ultraviolet lasers that hold important applications from high-resolution bio-imaging and laser therapy to optical storage [27]. Other paths are explored, like doping $CsPbCl_3$ quantum dots with paramagnetic transition metal Mn^{2+} ions and opening new potentialities to exciton energy transfer and electro-optical and magnetic properties for this material [28–30].

In this study, we implement low-temperature transmission spectroscopy in pulsed magnetic fields up to 68 T, giving direct access to the basic exciton parameters, such as binding energy of

the neutral free exciton and the excitonic reduced effective mass, μ, for $CsPbCl_3$ films. We found a large exciton binding energy and a weak effective mass, making $CsPbCl_3$ suitable for RT laser and polaritonic condensation applications.

2. EXPERIMENTAL RESULTS

$CsPbCl_3$ perovskite films were grown on a muscovite mica substrate using the chemical vapor deposition method described in previous works [25,31–33]. The growth mechanism is known as van-der-Waals epitaxy and needs substrates, such as mica, whose surfaces are inert due to the predominant absence of dangling bonds.

A typical optical microscopy image of grown films is shown in Fig. 1(a). The film thickness is in the 200–300 nm range. We observe strongly elongated parallelepipedal shaped domains with lateral dimensions of several tens of micrometers (μm).

Figure 1(b) shows the optical transmission of $CsPbCl_3$ films obtained at low temperature, 2 K, and zero magnetic field. Two minima are observed in the range 2.9 to 3.2 eV. These two minima correspond to the hydrogen-like exciton states $n = 1$ and 2, respectively, at 2.992 eV and 3.040 eV. Assuming a hydrogenic model for the exciton, we can write the energy of the nth exciton state as a function of the band gap energy, E_g, and the exciton binding energy, E_X, as follows:

$$E_n = E_g - \frac{E_X}{n^2}, \tag{1}$$

where $E_X = \frac{\mu e^4}{2(4\pi\varepsilon_0\varepsilon_r\hbar)^2} = E_H \frac{\mu}{m_0\varepsilon_r^2}$ with e the elementary charge, $\mu = (m_e m_h)/(m_e + m_h)$ the exciton effective mass, $m_{e(h)}$ is the electron (hole) effective mass, m_0 is the free electron mass, $\hbar$ is the reduced Planck's constant, ε_0 is the vacuum permittivity, ε_r is the relative permittivity experienced by the exciton, and $E_H = 13.605$ eV is the binding energy for the hydrogen atom. We deduce $E_X = 64 \pm 1.5$ meV from $E_2 - E_1 = 3E_X/4 = 48 \pm 1$ meV. This value is in good agreement with those calculated by discrete Fourier transform (DFT) methods [34] and experimental determinations [35,36]. Finally, from the energy position of the first minimum in the transmission spectrum, we obtain the energy gap for $CsPbCl_3$: $E_g = 3.056$ eV. Figure 1(c) shows the optical transmission of $CsPbCl_3$ films obtained at RT by using a PerkinElmer Lambda 950 UV-visible near-infrared (UV-VIS-NIR) spectrometer. Only one minimum is observed at RT corresponding to the ground-state exciton transition in agreement with the obtained binding energy of 64 meV, which is larger than the thermal energy at RT. The minimum appears at higher energy than the one observed at 2 K, 3.035 eV instead of 2.992 eV, and it is also broader.

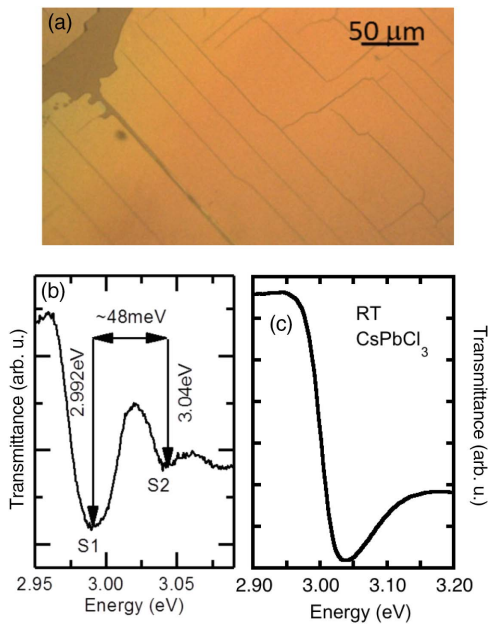

Fig. 1. (a) Typical optical microscopy (reflection configuration) image of a $CsPbCl_3 \sim 250$ nm thick film grown on muscovite mica following the method reported in Refs. [32,33]. (b) Optical transmittance of the film shown in (a) at 2 K and zero magnetic field. S_1 and S_2 correspond, respectively, to the $n = 1$ and 2 exciton states in the hydrogenic model. (c) Optical transmittance of the film shown in (a) at RT.

E_X is given in Table 1 and compared with the experimental values obtained in other organic and inorganic halide perovskite materials by using the same experimental method. A discussion is included below concerning data in Table 1 and Fig. 3.

Transmission measurements obtained at 2 K in high-magnetic fields are shown in Fig. 2(a). These measurements were performed in a Faraday configuration with pulsed magnetic fields up to 68 T (pulse duration 500 ms) in Toulouse at the Laboratoire National des Champs Magnétiques Intenses (LNCMI). An optical fiber was used to deliver white light from a xenon lamp. The focusing spot radius was 100–200 μm, allowing for the excitation of several domains. The circular polarization was introduced *in situ*. Rotation between σ^+ and σ^- polarized light was done by changing the magnetic field direction. The transmitted light was reflected back into a collecting fiber and a spectrometer equipped with a nitrogen cooled CCD detector, which was synchronized to the magnetic field pulse.

In a magnetic field, the exciton energy is modified and can be written as

$$E_{\pm}^n = E_0^n \pm \frac{1}{2} g_{\text{eff}} \mu_B B + \sigma_X^n B^2, \tag{2}$$

Table 1. Exciton Parameters in the Family of Halide Perovskite Compounds Deduced from Magneto-Optical Experiments at 2 K[a]

Compound	E_g (eV)	E_X (meV)	m_0	ε_r	g_{eff}
[b]$CsPbCl_3$	3.056	64 ± 1.5	0.202 ± 0.01	6.56 ± 0.24	0.8
[c]$CsPbBr_3$	2.342	33 ± 1	0.126 ± 0.01	7.3	
[c]$CsPbI_3$	1.723	15 ± 1	0.114 ± 0.01	10.0	
[d]$FAPbBr_3$	2.233	22	0.115	8.42	
[d]$FAPbI_3$	1.501	14	0.09	9.35	2.3
[d]$MAPbBr_3$	2.292	25	0.117	7.5	
[d]$MAPbI_3$	1.652	16	0.104	9.4	[e]1.2

[a]$CH_3NH_3^+$ = MA (methylammonium) or $CH(NH_2)_2^+$ = FA (formamidinium).
[b]This work.
[c]Reference [37].
[d]Reference [38].
[e]Reference [39].

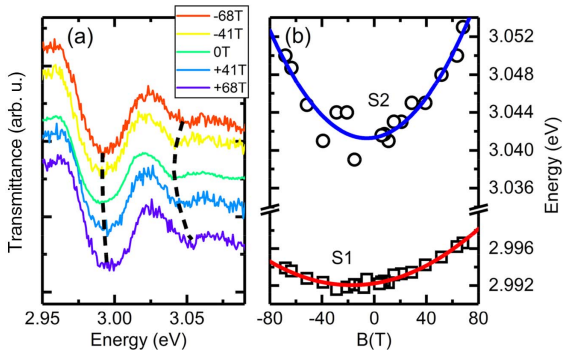

Fig. 2. (a) Optical transmittance of the $CsPbCl_3$ film shown in Fig. 1(a) at 2 K for different magnetic field values. The pulsed magnetic field is perpendicular to the film (Faraday configuration). (b) The energy position of S_1 ($n = 1$) and S_2 ($n = 2$) versus magnetic field. Parabolic fits to the data according to Eq. (2) in the main text lead to $g_{\text{eff}} = 0.8$ and diamagnetic shift coefficients σ_X^n of 0.64 μeV/T^2 and 2.0 μeV/T^2 for $n = 1$ and 2, respectively.

where E_0^n is the unperturbed energy of the nth exciton state, g_{eff} is the effective exciton Landé factor, μ_B is the Bohr magneton, B is the magnetic field amplitude, and σ_X^n is the diamagnetic shift coefficient. The second term in Eq. (2) is the linear Zeeman splitting induced by the application of a magnetic field that lifts the exciton states degeneracy, and the third term represents the diamagnetic shift that grows quadratically with the field amplitude (in the so-called low-field limit).

Fitting simultaneously the energy position of the $n = 1$ and 2 states by Eq. (2), we determine the exciton g factor $g_{\text{eff}} = 0.8$ and the diamagnetic shift coefficients $\sigma_X^1 = 0.64 \pm 0.05$ μeV/T^2 and $\sigma_X^2 = 2.0 \pm 0.2$ μeV/T^2. The diamagnetic shifts are significantly lower than those reported for lower band gap perovskites [22,37], which is a natural consequence of a higher exciton binding energy and lower Bohr radius for $CsPbCl_3$. Additionally the g factor is significantly lower than in case of I or bromide-based perovskite.

When the cyclotron energy is significantly smaller than the exciton binding energy, σ_X^1 can be written as a function of the effective exciton mass and the dielectric constant, as follows:

$$\sigma_X^1 = \frac{(4\pi\varepsilon_0\varepsilon_r)^2\hbar^4}{4\mu^3 e^2} = \sigma_H \frac{\varepsilon_r^2}{(\mu/m_0)^3}. \tag{3}$$

$\sigma_H = 1.231 \times 10^{-4}$ μeV/T^2 is the diamagnetic shift for the hydrogen atom. Combining the expressions of E_X and σ_X, we can obtain the exciton reduced mass and the relative permittivity of $CsPbCl_3$ as follows:

$$\frac{\mu}{m_0} = \sqrt{\frac{\sigma_H}{\sigma_X}\frac{E_H}{E_X}}, \tag{4}$$

$$\varepsilon_r = \left(\frac{\sigma_H}{\sigma_X}\frac{E_H^3}{E_X^3}\right)^{1/4}. \tag{5}$$

We then obtain $\frac{\mu}{m_0} = 0.202 \pm 0.010$ and $\varepsilon_r = 6.56 \pm 0.24$. Note that, by using the numerical calculation of Makado *et al.* [40] for the hydrogenic states under magnetic field, it is possible to deduce the parameter $\gamma = \frac{\hbar\omega_c}{2E_X}$ at high field from the behavior of the $n = 1$ and 2 lines splitting. $\omega_c = \frac{eB}{\mu}$ is the exciton cyclotron frequency. One gets $\frac{\gamma}{B} = 4.56 \times 10^{-3}$ T^{-1}. With $E_X = 64$ meV, one obtains $\frac{\mu}{m_0} = 0.199$, which is in very good agreement with the mass deduced from the $n = 1$ state diamagnetic shift in the low-field regime.

The comparison of the exciton reduced mass, exciton binding energy, and effective dielectric screening for perovskites with different halides is presented in Fig. 3. The exciton binding energy increases with increasing band gap as in more conventional semiconductors (see also Fig. 4). At the same time, it can be seen that the effective exciton mass follows reasonably the prediction of a simple two-band $k \cdot p$ model, $\mu \propto E_g$ [22]. Recent DFT calculations have addressed the electron and hole mass determination in $CsPbX_3$ compounds and predicted a significant enhancement of the carrier effective mass when I or Br is exchanged by Cl due to weaker hybridization of halide orbitals with lead [34,42–44]. With the increase of the halide atom mass, the energetic position and space extension of s and p orbitals favor the overlap with the Pb^{2+} states, increasing the band dispersion and therefore decreasing the effective exciton mass when one moves from the lighter Cl to heavier Br and I atoms. This effect is especially visible in the valence band, which contains significant admixture of halide orbitals. While most of these theoretical studies have underestimated the exciton mass as compared to experimental measurements, an increase in the exciton mass has been predicted from iodide to

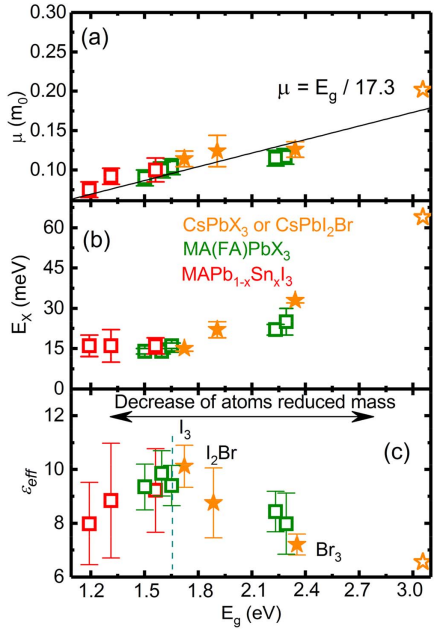

Fig. 3. (a) Exciton reduced mass, (b) exciton binding energy, and (c) effective dielectric constant as functions of the energy gap. Measurements are done at 2 K. Full orange stars correspond to $CsPbX_3$ with X = I, Br or to $CsPbI_2Br$ [37]. Empty orange stars correspond to $CsPbCl_3$ (this work). Open green squares represent results for the MA and formamindinium (FA) iodides, bromides, or mixed halide (green square at 1.596 eV is for $I_{3-x}Cl_x$) [38]. Open red squares correspond to $MAPb_{1-x}Sn_xI_3$ [41]. Black solid line in (a) is a linear fit to the data. Vertical dashed green line indicates the value of the energy gap at which a maximum of the effective dielectric constant is found for the considered perovskite compounds.

chloride, with a ratio of the exciton masses between 1.53 and 2.24. These predicted ratios are in agreement with the experimental value found in this study, leading to a ratio 0.202/0.114 = 1.77. Moreover, as observed in Table 1, organic and inorganic compounds with the same halide atom possess very similar exciton mass. Based on this observation, the comparison of our results with calculations on methyl ammonium lead chloride ($MAPbCl_3$) should be pertinent. Sendner *et al.* [45] have performed DFT calculations taking into consideration exchange-correlation functional and spin-orbit coupling and have predicted an exciton mass of $0.20m_0$ for $MAPbCl_3$ very similar to the one we measured in $CsPbCl_3$.

The dielectric screening is shown in Fig. 3(c). It follows the expected trend, i.e., at low temperature when the motion of cations is frozen, the metal halide cage is determined in the first approximation of the screening properties. The dielectric constant then decreases when the bromide or iodide is exchanged with lighter Cl atoms [37,41]. Such a substitution increases the energy of phonon modes [43], since this energy is proportional to the inverse of the reduced mass of atoms participating in the vibration. As we can see in Fig. 3(c), the substitution of Pb atoms by Sn atoms results also in a decrease of the dielectric screening. Then, Fig. 3(c) shows that the effective dielectric constant decreases as the reduced mass of atoms building the crystal decreases and, consequently, a non-monotonous behavior of the dielectric constant versus the energy gap of the considered perovskite compounds.

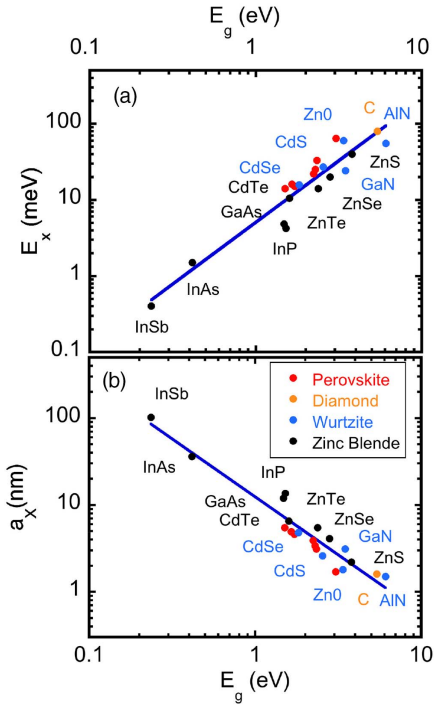

Fig. 4. (a) Exciton binding energy E_X and (b) Bohr radius a_X versus the gap energy of halide-based perovskites and other semiconductors with different crystalline structures, either zinc blende, wurtzite, or diamond. The solid lines correspond to fits with, respectively, $E_X \propto E_g^{1.62}$ and $a_X \propto E_g^{-1.33}$. Perovskite values are given in Table 1. InAs and ZnO [46], GaAs [47], ZnTe [48], ZnS [49], AlN [50], and the other semiconductors [51].

Putting together arguments given above and the latter discussion, we underline that the substitution of I^+ anions by Cl^+ increases the exciton binding energy in two ways, by increasing the carrier's effective mass and by reducing dielectric screening. We also see in Fig. 3(b) that when substituting the Pb^{2+} cation by Sn^{2+}, the exciton binding energy does not vary significantly. That is the result of a compensation of two effects: (i) the reduction of the effective mass that participates in the decrease of the exciton binding energy and (ii) the reduction of the dielectric screening that leads to the increase of the exciton binding energy.

To finish, we have compared the exciton binding energy E_X and the Bohr radius a_X of the halide-based perovskites with other semiconductor families, either those showing zinc blende, wurtzite, or diamond crystal structures. As shown in Fig. 4, the perovskite parameters follow the trends observed for other semiconducting crystals and phases in a large range of the band gap energy, with a large increase of E_X and decrease of a_X versus E_g. The solid lines correspond to least-square fits with $E_X \propto E_g^{1.62}$ and $a_X \propto E_g^{-1.33}$. As related previously, in a simple two-band model, $\mu \propto E_g$. Chadi and Cohen [52] have shown, at a large band gap energy, that the static dielectric constant follows the law $\varepsilon_r - 1 \propto a_0^{-1.5} E_g^{-1}$, with the lattice parameter a_0. At the same time, Dalven [53] has evidenced an empirical law $E_g \propto a_0^{-2}$ in a large band gap range. All of these laws lead to the relations $E_X \propto E_g^{1.5}$ and $a_X \propto E_g^{-1.25}$, with exponents very close to the ones obtained in Fig. 4.

3. CONCLUSION

We have performed a detailed magneto-optical study of the all-inorganic halide perovskite $CsPbCl_3$. The analysis of the transmission spectra obtained at low temperature and pulse magnetic field up to 68 T allows the determination of the crucial parameters to describe the exciton properties without assumption on the strength of the dielectric screening. This experimental approach is then self-consistent. We underline that the values of the exciton binding energy and effective mass increase with the band gap energy for the all-organic or inorganic perovskite compounds; meanwhile, the permittivity values have a non-monotonous behavior. The large exciton binding energy measured in $CsPbCl_3$ compounds makes them very promising materials for opto-electronic and polaritonic applications at RT.

Funding. Ministry of Education—Singapore (MOE2018-T2-2-068, MOE2018-T3-1-002, RG103/15 and RG113/16); National Science Centre Poland (OPUS 2019/33/B/ST3/01915); Agence Nationale de la Recherche (ANR- 18-CE30-0023-01, ANR-10-LABX-0037-NEXT).

Disclosures. The authors declare no conflicts of interest.

REFERENCES

1. H. Zhou, Q. Chen, G. Li, S. Luo, T.-B. Song, H.-S. Duan, Z. Hong, J. You, Y. Liu, and Y. Yang, "Interface engineering of highly efficient perovskite solar cells," Science **345**, 542–546 (2014).
2. W. S. Yang, J. H. Noh, N. J. Jeon, Y. C. Kim, S. Ryu, J. Seo, and S. Il Seok, "High-performance photovoltaic perovskite layers fabricated through intermolecular exchange," Science **348**, 1234–1237 (2015).

3. NREL, "Best-research-cell efficiencies," https://www.nrel.gov/pv/assets/pdfs/best-research-cell-efficiencies.20200406.pdf (2020).
4. S. D. Stranks and H. J. Snaith, "Metal-halide perovskites for photovoltaic and light-emitting diodes," Nat. Nanotechnol. **10**, 391–402 (2015).
5. B. R. Sutherland and E. H. Sargent, "Perovskite photonic sources," Nat. Photonics **10**, 295–302 (2016).
6. Q. Zhang, S. T. Ha, X. Liu, T. C. Sum, and Q. Xiong, "Room-temperature near-infrared high *Q* perovskite whispering-gallery planar lasers," Nano Lett. **14**, 5995–6001 (2014).
7. K. Lin, J. Xing, L. N. Quan, F. Pelayo Garcia de Arquer, X. Gong, J. Lu, L. Xie, W. Zhao, D. Zhang, C. Yan, W. Li, X. Liu, Y. Lu, J. Kirman, E. H. Sargent, Q. Xiong, and Z. Wei, "Perovskite light-emitting diodes with external quantum efficiency exceeding 20 percent," Nature **562**, 245–248 (2018).
8. L. T. Dou, Y. (Micheal) Yang, J. B. You, Z. R. Hong, W. H. Chang, G. Li, and Y. Yang, "Solution-processed hybrid perovskite photodetectors with high detectivity," Nat. Commun. **5**, 5404 (2014).
9. R. Su, C. Diederichs, J. Wang, T. C. H. Liew, J. Zhao, S. Liu, W. Xu, Z. Chen, and Q. Xiong, "Room-temperature polariton lasing in all-inorganic perovskites nanoplatelets," Nano Lett. **17**, 3982–3988 (2017).
10. P. Bouteyre, H. S. Nguyen, J. S. Lauret, G. Trippe-Allard, G. Delport, F. Ledee, H. Diab, A. Belarouci, C. Seassal, D. Garrot, F. Bretenaker, and E. Deleporte, "Room-temperature cavity polaritons with 3D hybrid perovskite: toward large-surface polaritonic devices," ACS Photon. **6**, 1804–1811 (2019).
11. S. Zhang, J. Chen, J. Shi, L. Fu, W. Du, X. Sui, Y. Mi, Z. Jia, F. Liu, J. Shi, X. Wu, N. Tang, Q. Zhang, and X. Liu, "Trapped exciton-polariton condensate by spatial confinement in a perovskite microcavity," ACS Photon. **7**, 327–337 (2020).
12. R. Su, J. Wang, J. Zhao, J. Xing, W. Zhao, C. Diederichs, T. C. H. Liew, and Q. Xiong, "Room temperature long-range coherent exciton polariton condensate flow in lead halide perovskites," Sci. Adv. **4**, eaau0244 (2018).
13. R. Sui, S. Ghosh, J. Wang, S. Liu, C. Diederichs, T. C. H. Liew, and Q. Xiong, "Observation of exciton polariton condensation in perovskite lattice at room temperature," Nat. Phys. **16**, 301–306 (2020).
14. Y.-S. Park, S. Guo, N. S. Makarov, and V. I. Klimov, "Room temperature single-photon emission from individual perovskite quantum dots," ACS Nano **9**, 10386–10393 (2015).
15. F. Hu, H. Zhang, C. Sun, C. Yin, B. Lv, C. Zhang, W. W. Yu, X. Wang, Y. Zhang, and M. Xiao, "Superior optical properties of perovskite nanocrystals as single photon emitters," ACS Nano **9**, 12410–12416 (2015).
16. C. Huo, C. F. Fong, M. R. Amara, Y. Huang, B. Chen, H. Zhang, L. Guo, H. Li, W. Huang, C. Diederichs, and Q. Xiong, "Optical spectroscopy of single colloidal $CsPbBr_3$ perovskite nanoplatelets," Nano Lett. **20**, 3673–3680 (2020).
17. Z. G. Yu, "Effective-mass model and magneto-optical properties in hybrid perovskites," Sci. Rep. **6**, 28576 (2016).
18. J. Ramade, L. M. Andriambariarijaona, V. Steinmetz, N. Goubet, L. Legrand, T. Barisien, F. Bernardot, C. Testelin, E. Lhuillier, A. Bramati, and M. Chamarro, "Fine structure of excitons and electron-hole exchange energy in polymorphic $CsPbBr_3$ single nanocrystals," Nanoscale **10**, 6393–6401 (2018).
19. P. C. Sercel, J. L. Lyons, D. Wickramaratne, R. Vaxenburg, N. Bernstein, and A. L. Efros, "Exciton fine structure in perovskite nanocrystals," Nano Lett. **19**, 4068–4077 (2019).
20. R. Ben Aich, I. Saïdi, S. Ben Radhia, K. Boujdaria, T. Barisien, L. Legrand, F. Bernardot, M. Chamarro, and C. Testelin, "Bright-exciton splittings in inorganic cesium lead halide perovskite nanocrystals," Phys. Rev. Appl. **11**, 034042 (2019).
21. R. Ben Aich, S. Ben Radhia, K. Boujdaria, M. Chamarro, and C. Testelin, "Multiband k·p model for tetragonal crystals: application to hybrid halide perovskite nanocrystals," J. Phys. Chem. Lett. **11**, 808–817 (2020).
22. M. Baranowski, K. Galkowski, A. Surrente, J. Urban, L. Klopotowski, S. Mackowsk, D. K. Maude, R. Ben Aich, K. Boujdaria, M. Chamarro, C. Testelin, P. K. Nayak, M. Dollmann, H. J. Snaith, R. J. Nicholas, and P. Plochocka, "Giant fine structure splitting of the bright exciton in a bulk $MAPbBr_3$ single crystal," Nano Lett. **19**, 7054–7061 (2019).
23. L. Q. Phuong, Y. Yamada, M. Nagai, N. Maruyama, A. Wakamiya, and Y. Kanemitsu, "Free carriers versus excitons in $CH_3NH_3PbI_3$ perovskite thin films at low temperatures: charge transfer from the orthorhombic phase to the tetragonal phase," J. Phys. Chem. Lett. **7**, 2316–2321 (2016).
24. P. Odenthal, W. Talmadge, N. Gundlach, R. Wang, C. Zhang, D. Sun, Z. G. Yu, Z. V. Vardeny, and Y. S. Li, "Spin-polarized exciton quantum beating in hybrid organic-inorganic perovskites," Nat. Phys. **13**, 894–900 (2017).
25. Q. Zhang, R. Su, X. Liu, J. Xing, T. C. Sum, and Q. Xiong, "High-quality whispering-gallery-mode lasing from cesium lead halide perovskite nanoplatelets," Adv. Funct. Mater. **26**, 6238–6245 (2016).
26. X. X. He, P. Liu, H. H. Zhang, Q. Liao, J. N. Yao, and H. B. Fu, "Patterning multicolored microdisk laser arrays of cesium lead halide perovskite," Adv. Mater. **29**, 1604510 (2017).
27. M. H. Huang, S. Mao, H. Feick, H. Yan, Y. Wu, H. Kind, E. Weber, R. Russo, and P. Yang, "Room-temperature ultraviolet nanowire nanolasers," Science **292**, 1897–1899 (2001).
28. W. Liu, Q. Lin, H. Li, K. Wu, I. Robel, J. M. Pietryga, and V. I. Klimov, "Mn^{2+}-doped lead halide perovskite nanocrystals with dual-color emission controlled by halide content," J. Am. Chem. Soc. **138**, 14954–14961 (2016).
29. D. Parobek, B. J. Roman, Y. Dong, H. Jin, E. Lee, M. Sheldon, and D. H. Son, "Exciton-to-dopant energy transfer in Mn-doped cesium lead halide perovskite nanocrystals," Nano Lett. **16**, 7376–7380 (2016).
30. X. Yuan, S. H. Ji, M. C. De Siena, L. L. Fei, Z. Zhao, Y. J. Wang, H. B. Li, J. L. Zhao, and D. R. Gamelin, "Photoluminescence temperature dependence, dynamics, and quantum efficiencies in Mn^{2+}-doped $CsPbCl_3$ perovskite nanocrystals with varied dopant concentration," Chem. Mater. **29**, 8003–8011 (2017).
31. K. Saiki, K. Ueno, T. Shimada, and A. Koma, "Application of van-der-Waals epitaxy to highly heterogeneous systems," J. Cryst. Growth **95**, 603–606 (1989).
32. M. I. Utama, Z. Peng, R. Chen, B. Peng, X. Xu, Y. Dong, L. M. Wong, S. Wang, H. Sun, and Q. Xiong, "Vertically aligned cadmium chalcogenide nanowire arrays on muscovite mica: a demonstration of epitaxial growth strategy," Nano Lett. **11**, 3051–3057 (2011).
33. S. T. Ha, X. Liu, Q. Zhang, D. Giovanni, T. C. Sum, and Q. Xiong, "Synthesis of organic-inorganic lead halide perovskite nanoplatelets: towards high-performance perovskite solar cells and optoelectronic devices," Adv. Opt. Mater. **2**, 838–844 (2014).
34. L. Protesescu, S. Yakunin, M. I. Bodnarchuk, F. Krieg, R. Caputo, C. H. Hendon, R. Xi Yang, A. Walsh, and M. V. Kovalenko, "Nanocrystals of cesium lead halide perovskites ($CsPbX_3$, X = Cl, Br, and I): novel optoelectronic materials showing bright emission with wide color gamut," Nano Lett. **15**, 3692–3696 (2015).
35. H. Ito, J. Nakahara, and R. Onaka, "Magneto-optical study of the exciton states in $CsPbCl_3$," J. Phys. Soc. Jpn. **47**, 1927–1935 (1979).
36. D. Fröhlich, K. Heidrich, and G. Trendel, "Cesium-trihalogen-plumbates a new class of ionic semiconductors," J. Lumin. **18-19**, 385–388 (1979).
37. Z. Yang, A. Surrente, K. Galkowski, A. Miyata, O. Portugall, R. J. Sutton, A. A. Haghighirad, H. J. Snaith, D. K. Maude, P. Plochocka, and R. J. Nicholas, "Impact of the halide cage on the electronic properties of fully inorganic cesium lead halide perovskites," ACS Energy Lett. **2**, 1621–1627 (2017).
38. K. Galkowski, A. Mitioglu, A. Miyata, P. Plochocka, O. Portugall, G. E. Eperon, J. Tse-Wei Wang, T. Stergiopoulos, S. D. Stranks, H. J. Snaith, and R. J. Nicholas, "Determination of the exciton binding energy and effective masses for methylammonium and formamidinium lead tri-halide perovskite semiconductors," Energy Environ. Sci. **9**, 962–970 (2016).
39. M. Hirasawa, T. Ishihara, T. Goto, K. Uchida, and N. Miura, "Magnetoabsorption of the lowest exciton in perovskite-type compound $(CH_3NH_3)PbI_3$," Physica B **201**, 427–430 (1994).
40. P. C. Makado and N. C. McGill, "Energy level of a neutral hydrogen-like system in a constant magnetic field of arbitrary strength," J. Phys. C **19**, 873–885 (1986).
41. K. Galkowski, A. Surrente, M. Baranowski, B. Zhao, Z. Yang, A. Sadhanala, S. Mackowski, S. D. Stranks, and P. Plochocka,

"Excitonic properties of low-band-gap lead–tin halide perovskites," ACS Energy Lett. **4**, 615–620 (2019).
42. M. A. Becker, R. Vaxenburg, G. Nedelcu, P. C. Sercel, A. Shabaev, M. J. Mehl, J. G. Michopoulos, S. G. Lambrakos, N. Bernstein, J. L. Lyons, T. Stöferle, R. F. Mahrt, M. V. Kovalenko, D. J. Norris, G. Rainò, and A. L. Efros, "Bright triplet excitons in caesium lead halide perovskites," Nature **553**, 189–193 (2018).
43. Y. Kang and S. Han, "Intrinsic carrier mobility of cesium lead halide perovskites," Phys. Rev. Appl. **10**, 044013 (2018).
44. S. T. A. G. Melissen, F. Labat, P. Sautet, and T. Le Bahers, "Electronic properties of $PbX_3CH_3NH_3$ (X=Cl, Br, I) compounds for photovoltaic and photocatalytic applications," Phys. Chem. Chem. Phys. **17**, 2199–2209 (2015).
45. M. Sendner, P. K. Nayak, D. A. Egger, S. Beck, C. Muller, B. Epding, W. Kowalsky, L. Kronik, H. J. Snaith, A. Pucci, and R. Lovrincic, "Optical phonons in methylammonium lead halide perovskites and implications for charge transport," Mater. Horiz. **3**, 613–620 (2016).
46. B. Guzelturk, P. L. Hernandez Martinez, Q. Zhang, Q. Xiong, H. Sun, X. W. Sun, A. O. Govorov, and H. V. Demir, "Excitonics of semiconductor quantum dots and wires for lighting and displays," Laser Photon. Rev. **8**, 73–93 (2014).
47. D. D. Sell, S. E. Stokowski, R. Dingle, and J. V. DiLorenzo, "Polariton reflectance and photoluminescence in high purity GaAs," Phys. Rev. B **7**, 4568–4586 (1973).
48. C. Neumaon, A. Notheand, and N. O. Lipari, "Two-photon magneto-absorption of ZnTe, CdTE and GaAs," Phys. Rev. B **37**, 922–932 (1988).
49. T. K. Tran, W. Park, W. Tong, M. M. Kyi, B. K. Wagner, and C. J. Summers, "Photoluminescence properties of ZnS epilayers," Appl. Phys. Lett. **81**, 2803–2809 (1997).
50. E. Silveira, J. A. Freitas, M. Kneissl, D. W. Treat, N. M. Johnson, G. A. Slack, and L. J. Schowalter, "Near-bandedge cathodoluminescence of an AlN homoepitaxial film," Appl. Phys. Lett. **84**, 3501–3503 (2004).
51. H. Warlimont and W. Martienssen, *Springer Handbook of Materials Data*, 2nd ed. (Springer, 2018).
52. D. J. Chadi and M. L. Cohen, "Correlation between the static dielectric constant and the minimum energy gap," Phys. Lett. A **49**, 381–382 (1974).
53. R. Dalven, "Empirical relation between energy gap and lattice constant in cubic semiconductor," Phys. Rev. B **8**, 6033–6034 (1973).